Journal of Electroanalytical Chemistry 832 (2019) 343–352

Contents lists available at ScienceDirect

Journal of Electroanalytical Chemistry

journal homepage: www.elsevier.com/locate/jelechem

Engineering and understanding of synergistic effects in the interfaces of rGO-CNTs/PtPd nanocomposite revealed fast electro-oxidation of methanol

Ammar Bin Yousaf[a,*], M. Imran[b], Syed Javaid Zaidi[a], Peter Kasak[a,*]

[a] Center for Advanced Materials, Qatar University, Doha 2713, Qatar
[b] Division of Nanomaterials and Chemistry, Hefei National Laboratory for Physical Sciences at Microscale, University of Science and Technology of China, Hefei 230026, China

ARTICLE INFO

Keywords:
Nanocomposites
Synergism
Electrocatalysts
Methanol oxidation reaction
Energy conversion

ABSTRACT

The developing human societies are being faced provoking energy crises due to higher demands of energy for increasing worldwide populations. The massive depletion of natural resources and global warming issues sound a laud alarm for modern societies. Methanol is attracting huge attractions as an alternative fuel in direct methanol fuel cells for the development of future energy conversion resources, while the fast chemisorptions of methanol and stable performance remained a challenge thereby hampering their scalable applications at commercial level. Herein, we focused on these goals by alteration in chemistry of materials being used as anode catalysts for direct methanol fuel cells. The promising PtPd alloy nanoparticles with tailored compositions are loaded on highly conductive rGO-CNTs support material. The highly active components of the metals and powerful electron transfer material as a support, these combined characteristics in one nanostructure facilitate the fast chemisorptions of methanol with durable performance. The ex-situ electrochemical and in-situ online differential electrochemical mass spectrometric analysis reveal the enhanced electrocatalytic methanol oxidation reaction activities attribute towards direct chemisorptions intermediate pathways introduced via geometric and structural factor within nanocomposite material.

1. Introduction

Direct methanol fuel cells (DMFCs) have been proved to be highly promising power generators for energy alternative devices because of their high energy density, convenient fuel storage and environment friendly nature [1–5]. Catalysts play a role of pillars in DMFCs due to the sluggish kinetics of the methanol chemisorptions at the anode. To date, number of strategies has been adopted to improve the performance of methanol oxidation reactions (MOR) catalysts. Among those, tailoring of geometries and chemistry of materials for monometallic, bimetallic and multimetallic catalysts involved. Pt has been widely used monometallic catalysts for MOR because of its promising performance [6,7]. However, due to substantial drawbacks correlating with high cost of the platinum being precious metal and loss of electrocatalytic activity by poisoning of its active sites strongly reduces durability of DMFCs which hinder their commercialization over large-scale [8–10].

Alloying Pt with less expensive noble metals such as Pd, Ag, Au and Ru is an effective approach to reduce the catalyst poisoning issues and enhances its electrocatalytic activity, accompanied by decreasing the consumption of Pt active sites [11–13]. Among above, Pd shown better partnership with Pt by facilitating the dissociation of water molecules and adsorption of MOR intermediates species outshine the other noble metals. Although great progress has been made in this combination, the enhanced activity, durability and stability of PtPd alloys for MOR still need to be improved [14]. As inside the catalyst chemistry, the support material plays important role via transference of electrons to improve the performance of overall catalyst synergistically. The choice of effective support material has been criterion among the factors such as having strong affinity with catalyst particles to stabilize them, owning a high surface area and a high electrical conductivity to promote fast electron transfer in redox reactions with corrosion resistant behavior under the operating conditions [15–17].

In near decade, carbon nanotubes (CNTs) and graphene oxide (GO) have been extensively used to fabricate the metals in constituting the effective catalyst materials. The combination of rGO sheets and carbon nanotubes (CNTs) has also shown its excellent performance in energy application devices due to exceptional properties of both the materials [18–21]. The functional groups on GO makes it favorable to incorporate in composite form with other functional nanomaterials with sp^2-bonded aromatic carbon regions [22,23]. Also the oxygen-containing functional

* Corresponding authors.
E-mail addresses: ammar@mail.ustc.edu.cn (A.B. Yousaf), peter.kasak@qu.edu.qa (P. Kasak).

https://doi.org/10.1016/j.jelechem.2018.11.033
Received 23 August 2018; Received in revised form 14 November 2018; Accepted 19 November 2018
Available online 20 November 2018

groups make GO hydrophilic, while the aromatic regions offer active sites to facilitate interaction with other carbon-based aromatic molecules through π–π supramolecular chemistry [24,25]. Whereas, CNTs can bridge the defects for mutual electron transfer phenomenon and effectively prevent the restacking or aggregation of rGO sheets. Moreover, unusual intercalation properties, corrosion resistant behavior and high chemical stability of CNTs make them auspicious in overall composite material [26].

Recently, Liu et al. [27] and Zhan et al. [28] have tuned PdPt alloys fabricated on carbon black and tested for MOR catalysis, Kim et al. [29] and Yang et al. [30] incorporated PdPt alloys on rGO and CNTs respectively for methanol electro-oxidation. These groups have tried different composition with tuned synthetic strategies to get MOR catalysts with optimal performance. Therefore, the sluggish of MOR kinetics remained a challenging task to overcome. So far, the loading of PtPd auspicious couple on highly active rGO-CNTs composite support have not been tested for methanol electro-oxidation. Herein, we have developed a unique electrocatalyst consisting of PtPd alloys supported on rGO-CNTs composite which were tested for MOR in an acidic medium. The precisely synthesized capping agent free catalyst has shown enhanced electro-oxidation of methanol which was revealed by online differential electrochemical mass spectrometry (DEMS). Strong MOR characterizing tool, the online DEMS has shown fast chemisorptions of methanol facilitating smooth six electrons transfer phenomenon by mutual interactions of carbon support and metallic alloys in electrocatalyst.

2. Experimental section

2.1. Reagents

Natural graphite powder and carbon nanotubes (CNTs) were purchased from Alfa Aesar. H_2PdCl_4 (99.9% metal basis) was from Alfa Aesar, K_2PtCl_6 (40%) was purchased from Fluka and CH_3OH (99.9%) was purchased from J.T. Baker. Other reagents were purchased from Sinopharm Chemical Reagent Co., Ltd. All reagents were of analytical-reagent grade.

2.2. Characterizations

The crystallographic structure, morphology and element compositions of the synthesized catalyst were studied by transmission electron microscopy (TEM), X-ray diffraction (XRD) and X-ray photoelectron spectroscopy (XPS). Transmission electron microscopic (TEM) images and high-resolution transmission electron microscopic (HRTEM) images were carried out on a JEM-2100F field emission electron microscope at an accelerating voltage of 200 kV. The X-ray powder diffraction (XRD) patterns of the samples were collected on a Rigaku/Max-3A X-ray diffractometer with Cu Kα radiation (λ = 1.54178 Å), the operation voltage and current was maintained at 40 kV and 200 mA, respectively. The X-Ray photoelectron spectroscopy (XPS) was performed at a Perkin-Elmer RBD upgraded PHI-5000C ESCA system.

2.3. Synthesis of PtPd/rGO-CNTs catalyst

The typical synthesis of PtPd/rGO-CNTs is a two step process. In the first step, rGO-CNTs composite support was synthesized as followed; the pre-functionalized GO (synthesized by modified Hummers and Offenmans method) [31,32] obtained and CNTs in an acidic medium for 5 h with stirring at elevated temperature were used for rGO-CNTs synthesis. These functionalized GO and CNTs were dispersed in Milli-Q water with a 3:1 ratio and sonicated for 2–3 h. Then the dispersion mixture was transferred into an autoclave and hydrothermally treated at 210 °C for 24 h in order to obtain the composite with three dimensional composite structures.

Afterwards in second step, PtPd alloy nanoparticles were loaded onto the surface of rGO-CNTs. The atomic compositions for PtPd were varied as 75:25, 50:50 and 25:75 for $Pt_{75}Pd_{25}$/rGO-CNTs, $Pt_{50}Pd_{50}$/rGO-CNTs and $Pt_{25}Pd_{75}$/rGO-CNTs catalysts respectively. Whereas, the cumulative weight percentage of both the metals PtPd was fixed as 6 wt % in all the catalysts and the composition of these two candidates was varied by changing the concentration of their precursors H_2PdCl_4 and K_2PtCl_6 followed to add in 50 mL of H_2O containing 1 mg/mL of rGO-CNTs. The suspension was stirred over night at room temperature, during this process the PtPd ions were supposed to adsorb over the carbon support material. The suspension was heated slowly at 60 °C to evaporate the water, and then obtained material was treated for calcinations in a furnace for 3 h at 350 °C in Ar/H_2 environment to reduce the Pt and Pd ions which were adsorbed at the surface. Resultantly, the homogeneous dispersed bimetallic alloys on rGO-CNTs were obtained. The final products were designated as $Pt_{75}Pd_{25}$/rGO-CNTs, $Pt_{50}Pd_{50}$/rGO-CNTs, $Pt_{25}Pd_{75}$/rGO-CNTs and further used for characterizations and applications. Similarly, monometallic Pt and Pd catalysts represented as $Pt_{100}Pd_0$/rGO-CNTs and Pt_0Pd_{100}/rGO-CNTs were prepared by the above same method.

2.4. Electrochemical measurements

Before each electrochemical experiment, a glassy carbon (GC) electrode (0.196 cm^2 geometric surface are) was first polished with alumina slurries (Al_2O_3, 0.05 mm) on a polishing cloth to obtain a mirror finish, followed by sonication in 0.1 M HNO_3, 0.1 M H_2SO_4, and pure water for 10 min, successively. To prepare a catalyst supported working electrode, 10 μL of 2 mg/mL suspension in ethanol was drop-coated on the polished electrode surface by a micro liter syringe, with a catalyst loading of 0.1 mg cm^{-2}, followed by drying in vacuum at room temperature. Afterwards, the catalyst was covered with a thin layer of Nafion (0.1 wt% in water, 5 μL) to ensure that the catalyst was tightly attached to the electrode surface during the electrochemical measurements. Voltammetry measurements were carried out with a CHI660D electrochemical workstation. The electrode prepared above was used as the working electrode. The Ag/AgCl (in 3 M KCl, aq.) combination, isolated in a double junction chamber and a Pt coil were used as the reference and counter electrodes, respectively. All the measurements were performed in electrochemical experiments with respect to the standard values of reversible hydrogen electrode (RHE). Electrochemical experimental work was done by potential cycling and chronoamperometric methods for MOR studies in 0.1 M $HClO_4$ + 1 M CH_3OH solution with N_2 purging at a scan rate of 50 mV s^{-1}. Whereas, the DEMS setup used in this study is a HidenHPR-40 DSA Bench top-membrane inlet gas analysis system, mass signals are collected 20 points/s. The mass signal for CO_2 produced has been calibrated by oxidative stripping of a saturated CO adlayer pre-adsorbed at 0.06 V, mass calibration constant $k = QF / Q$ mass is found to be 3.65×10^6 mA/Torr.

3. Results and discussions

The structural and morphological analysis for PtPd/rGO-CNTs electrocatalyst was carried out by transmission electron microscopy (TEM) and high magnification TEM (HRTEM) micrograph. The TEM micrograph for neat rGO-CNTs composite has taken before the loadings of PtPd alloys and compared with the TEM images after the alloys loadings to confirm the successful fabrication of catalyst material, shown in Fig. S1A & B. The real Pt and Pd loadings on rGO-CNTs support in all the catalysts were also analyzed by ICP-MS analysis to evaluate the difference between actual and nominal metals loadings. The detailed Pt and Pd molar and weight percentage (wt%) measurements for all the catalysts is provided in Table S1. The PtPd loading on rGO/CNTs was also evaluated by thermogravimetric analysis, taking into account the difference in TGA before and after metal loading. (see Fig. S2). The resulting values of the PtPd loading was 6 wt%, which are in agreement with experimental values. Moreover, inductively coupled

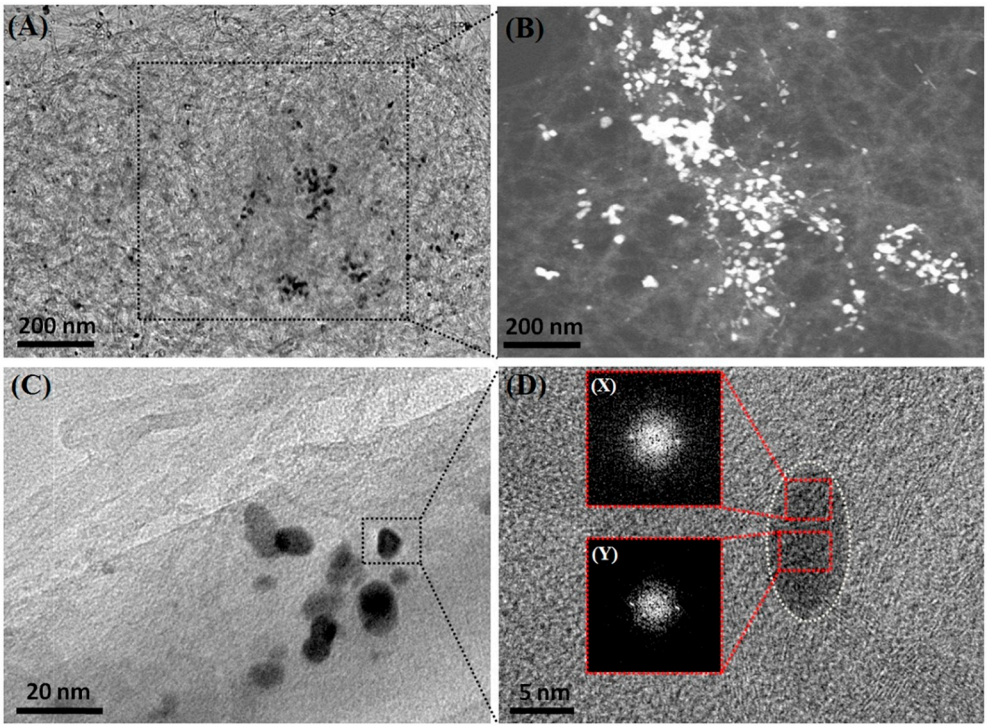

Fig. 1. TEM and HRTEM images of $Pt_{75}Pd_{25}$/rGO-CNTs catalyst. (A) Low magnification dark field TEM image of $Pt_{75}Pd_{25}$/rGO-CNTs catalyst, (B) low magnification bright field TEM image of $Pt_{75}Pd_{25}$/rGO-CNTs catalyst, (C) higher magnification TEM image of $Pt_{75}Pd_{25}$/rGO-CNTs catalyst and (D) HRTEM image of $Pt_{75}Pd_{25}$/rGO-CNTs catalyst, insets X & Y: FFT patterns of $Pt_{75}Pd_{25}$ bimetallic alloys extracted from HRTEM micrograph, showing the lattice fringes facets (111) shared by each element Pt & Pd in their alloy formation.

plasma mass spectrometry (ICP), also confirmed the validity of the TGA analysis for determination of PtPd loading (see Fig. S2).

The low-magnification TEM images have shown that successful loading of PtPd bimetallic alloys was done on rGO-CNTs support material with an average nanometric size of 7–9 nm, the dark tiny spheres representing the PtPd bimetallic alloys fabricated on rGO-CNTs (see Fig. 1A–C). The intimate contact of the encored bimetallic alloys with rGO-CNTs support channel were observed by high resolution transmission electron microscopy (HRTEM) analysis with their calculated standard specific crystal lattice signatures. The HRTEM results also indicate the successful formation of PtPd bimetallic nanosized alloys by sharing the same facets structure and almost identical lattice constant (with a mismatch of only 0.768%) comprising a bimetallic structures those are in contact with the rGO-CNTs support [33].

The bimetallic PtPd NPs exhibit the d-spacing values of 0.22 nm corresponding to the (111) planes of PtPd homogeneous phase (see Fig. 1D). In addition, the Fast Fourier transform (FFT) patterns (inset in Fig. 1D, Fig. X & Y) are also taken the calculation of lattice spacing values, giving a strong message of crystallite formation for as-developed material with (111) facets. Moreover, HAADF-STEM elemental mappings were also performed to examine the distribution of Pt and Pd in the bimetallic alloy particles (see Fig. 2A–E). These results strengthen the indication of PtPd alloy formation on the surfaces of rGO-CNTs, and both the metals have well homogeneous dispersion.

The structure and crystalline phase of prepared catalysts were measured by X-ray diffraction (XRD) patterns (see Fig. 3). The XRD diffraction patterns of Pd/rGO-CNTs catalyst, diffraction peaks ascribed to the Pd (111), (200), and (220) crystalline planes of the face centered cubic (fcc) structure of Pd are strongly coinciding with an fcc crystalline structure of bulk Pd (JCPDS, card no. 46-1043). Whereas, the XRD diffraction pattern of Pt are consisting with (JCPDS, card no 04-0802) and well-defined diffraction peaks observed, correspond to the (111), (200), (220), (311) and (222) crystal planes of fcc Pt in Pd/rGO-CNTs catalyst. In the XRD pattern of PtPd/rGO-CNTs, (111) peak is located at 2θ 40.10, considering the peak position of (111) more closely, it is evident that the peak position is moved from 39.76 to 40.10 in PtPd/rGO-CNTs by incorporating the Pd with Pt [34,35]. Thus, PtPd/rGO-CNTs also show Pt peaks of a polycrystalline fcc structure indexed to Pt (JCPDS, PDF # 04-0802). The patterns corresponding to the PtPd bimetallic sample showing the mixed features of Pt and Pd peak positions, hence the diffraction peaks for respective metal are shifted to higher angles compared with that of its monometallic existence, indicating the formation of an alloyed structure by incorporation of Pd into Pt in the bimetallic material. The diffraction peak values for (111) plane vary roughly linearly as a function of apparent composition in PtPd alloys. This trend clearly suggests the successful formation of PtPd alloys, resulting in an increase of the unit cell lattice parameter through an increase in the addition of Pd into Pt. The shifting of XRD peak positions to higher angles (111) peak at 40.72°, compared to the standard Pt XRD (111) at 39.76° (PDF # 04-0802), also indicating that Pd, with a relatively smaller atomic radius, is incorporated into the Pt lattice by sharing the same facet structures to form an alloy structure with a resulting lattice contraction. The ambiguity may be caused due to some overlapping peaks for rGO-CNTs and compared to other samples in which Pd is incorporated into the Pt lattice sharing the same facet structure. Consequently, the XRD patterns confirmed the association of ordered structure of the PtPd intermetallic phase. In addition, the peaks shakeup between 20° and 30° attribute towards carbon materials, the relatively broad diffraction peak observed at 25.85° corresponds to the (002) planes of graphene and the higher intensity peak at 27.11° correspond to the presence of CNTs along with rGO [36,37].

The X-ray photoelectron spectroscopy (XPS) studies of PtPd/rGO-CNTs catalyst were employed to investigate the information related to its surface chemistry. The full range survey spectrum contains signatures of all the expected metals such as, Pt, Pd and C at their corresponding binding energy positions (see Fig. 4A). The C1s XPS spectra provide the knowledge related to the reduction of surface groups. The results shown in Fig. 4B reveal there are three domains assigned to carbonyl groups (C═O) and C—O & C—C bonds and the π–π* [38,39]. The strong peak intensity associated with C—C bonds indicates that the sp^2-hybridized graphitic structure that is predominant domain among others also correspond the substantial reduction of oxygenated functional groups with fabrication of bimetallic alloys onto them. The high resolution Pt 4f deconvoluted spectrum with $4f_{5/2}$ and $4f_{7/2}$ doublets corresponding binding energies positions appeared at 74.53 eV and 71.35 eV, respectively, with an asymmetric nature, exhibit to the

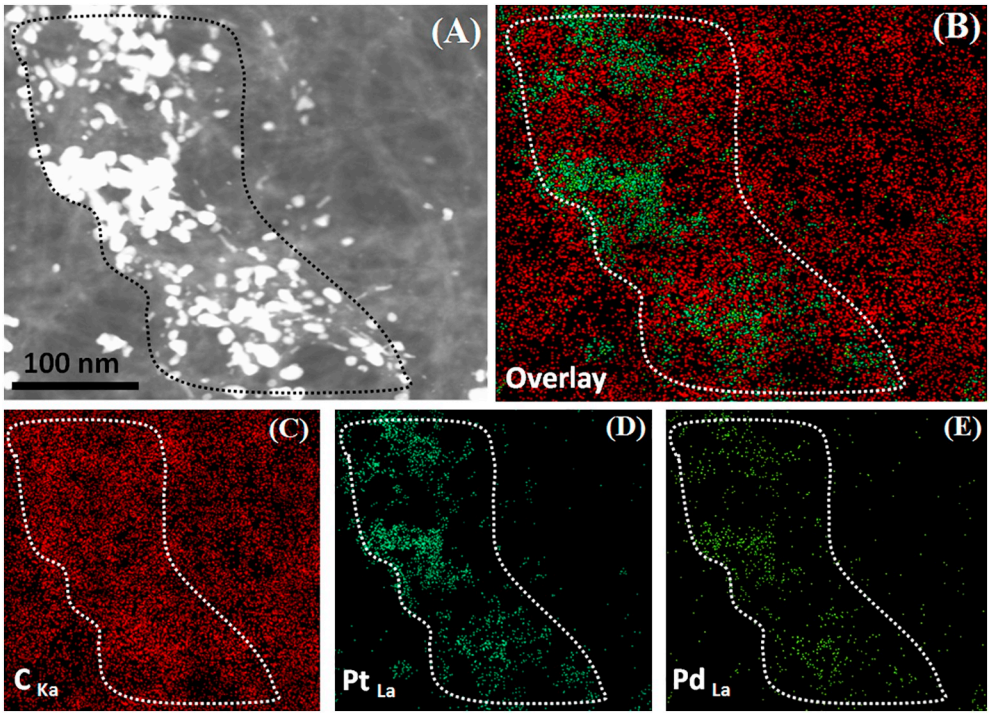

Fig. 2. HAADF-STEM element mapping images of $Pt_{75}Pd_{25}$/rGO-CNTs catalyst. (A) Selected area for HAADF-STEM element mapping measurements in dark field TEM image of $Pt_{75}Pd_{25}$/rGO-CNTs catalyst, (B) overlay representations for all the constituents C, Pt & Pd for the selected area of measurements and (C–E) HAADF-STEM element mapping of C, Pt & Pd respectively, in $Pt_{75}Pd_{25}$/rGO-CNTs catalyst.

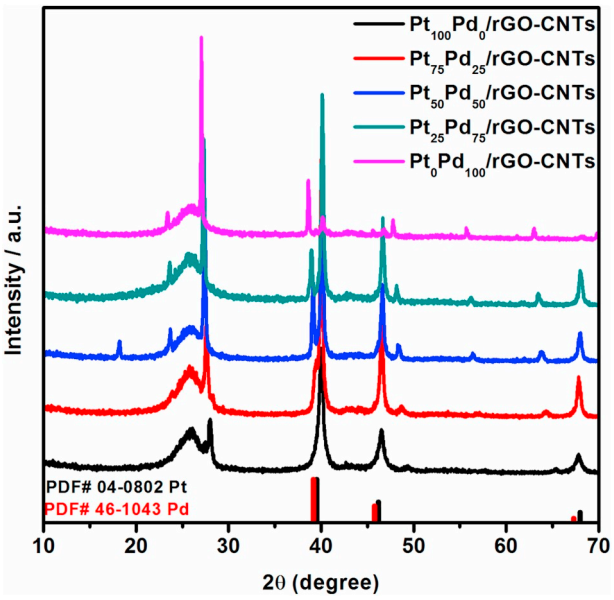

Fig. 3. XRD patterns for all the prepared series of PtPd alloys on rGO-CNTs support material.

relatively dominant metallic Pt(0) state (see Fig. 4C) [40]. Similarly, the Pd 3d wide range deconvoluted scan contains two spin-orbit doublets of $3d_{5/2}$ and $3d_{3/2}$ at 334.95 eV and 340.21 eV respectively, corresponding to the core electrons of metallic Pd(0) state (see Fig. 4D) [41]. It was observed that the predominant surface species in the prepared bimetallic catalysts are the metallic Pd states and relatively minor amounts of the oxidized species are also present, this shakeup in peaks is due to its contact with air. The electronic interaction between Pt and Pd was also examined by these XPS results.

The binding energy values of the metallic Pt for $4f_{7/2}$ domain peak are negatively shifted compared with its standard value (71.51 eV), which suggests that the electronic structure of Pt was modified by incorporation of Pd in PtPd bimetallic alloys. This shifting of binding energies towards lower values and significant electronic modifications in Pt structure predicts electron transference phenomenon from Pd to Pt in bimetallic alloys geometry. Whereas, the downshifting binding energies of Pt shows that Pd is donating electrons to Pt, following the substantial increase in the electron density around the Pt sites. Furthermore, this increase in electron density would favor for its methanol electro-oxidation performance by weaken the chemisorption of poisoning intermediate specie CO, hence consequently, improve the CO-poisoning issue in DMFCs, and facilitating the oxidation of methanol [42,43]. In addition, the binding energy values for Pd spin-orbit doublets are slightly shifted towards higher values than those of its standard peak positions relative to bulk Pd. Taking into account this shift in Pd peaks values towards higher BEs is also attributed to the strong interplay between Pd and rGO-CNTs support, furthermore, showing the existence of strong metals to support interactions [44]. Moreover, the electronic effects for Pt and Pt in bimetallic geometries can also be explained by means of electronegativity differences in relation with their shift of binding energies in XPS results. As discussed earlier, the shifting of binding energies of Pt and Pd relative to their standard values indicating the change in their electronic structures. These can be ascribed to the presence of electronic interactions between Pt and Pd atomic orbitals within the alloys. Hence, leading to electron transfer phenomenon from Pd to Pt due to the higher electronegativity of Pt, (2.28) compared to Pd (2.20). These electronic effect phenomena have also commonly seen in Pt-based alloys [45,46].

The cyclic voltammograms (CVs) curves for all the catalysts were recorded at room temperature in N_2 saturated 0.1 M $HClO_4$ aqueous solution at a scan rate of 50 mV s^{-1}. The characteristic CVs trends show the typical three components of electrochemical evaluation such as hydrogen adsorption/desorption region (H_{upd}), an electrochemical double-layer charging region and surface metal oxidation/reduction region, at between ca. 0.05–0.30 V, 0.40–0.75 V and above 0.90–0.95 V respectively, for all the catalysts in the positive scanning direction. Whereas, the negative scanning direction indicates the formation of a hydroxide layer (OH_{ad}) on the nanoparticles alloys surface. In this reverse direction curve, the two peaks attribute to surface reduction and hydrogen adsorption loops (see Fig. 5A). The diagnostic H_{upd} peaks

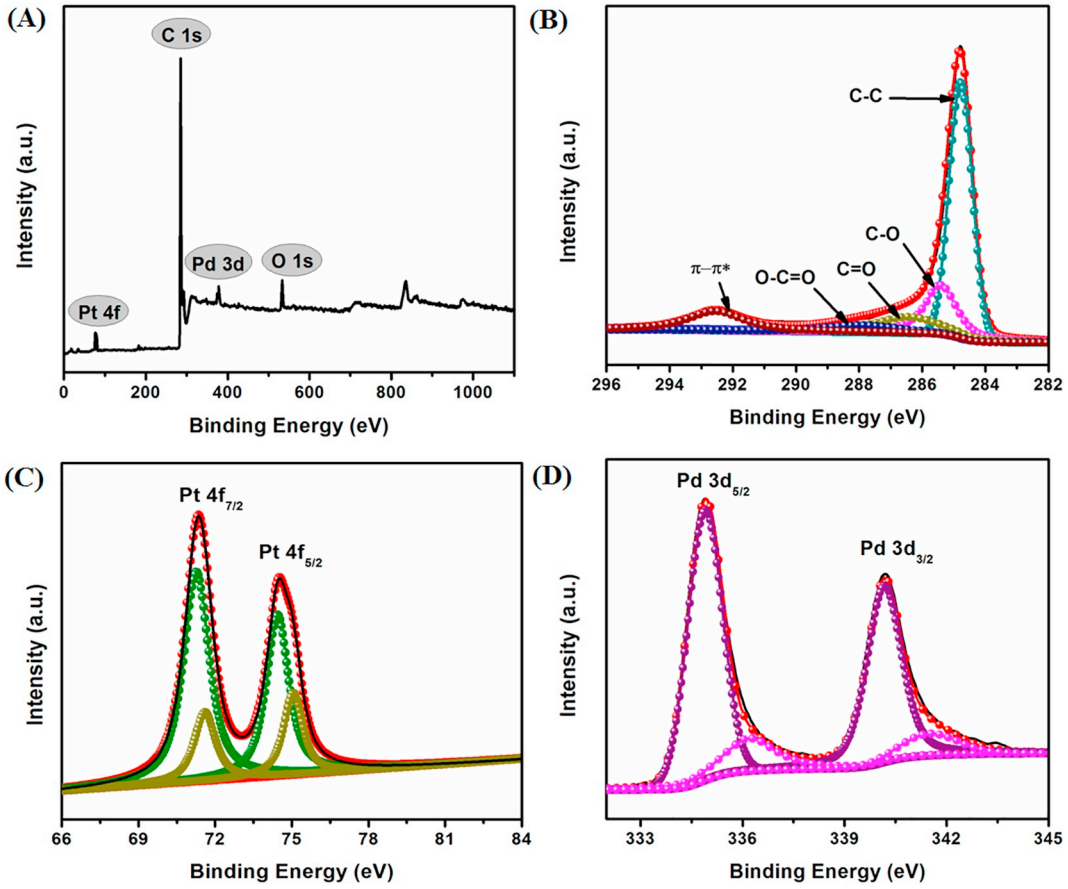

Fig. 4. XPS spectra of $Pt_{75}Pd_{25}$/rGO-CNTs catalyst. (A) The survey scan, representing the presence of each constituent element in $Pt_{75}Pd_{25}$/rGO-CNTs, (B) the C1s high resolution deconvoluted spectrum, (C) the Pt4f high resolution deconvoluted spectrum, (D) the Pd3d high resolution deconvoluted spectrum, within $Pt_{75}Pd_{25}$/rGO-CNTs catalyst.

with pure Pt proportion exhibit a combination of (100) and (111) facets of Pt sites terraces [47,48]. It can be seen from CV curves of PtPd bimetallic catalysts that the characteristic H_{upd} loops are located between pure Pt and Pd catalysts and exhibit negative shift in peak when the Pt proportion is increased (see inset Fig. 5A). The same shifting trend observed in the OH_{ad} peaks. As for the concern of Pd sites adsorption with $-OH_{ad}$ species, these are usually originate at a lower potential values than those of Pt-OH_{ad} species, this behavior is due to the fact that Pd is more vulnerable to oxidation. These scientific observations and reasoning confirm that Pt and Pd are strongly associated with each other in the PtPd bimetallic structures forming alloys materials [27,49].

These electrochemical characteristic furthers strongly supports the

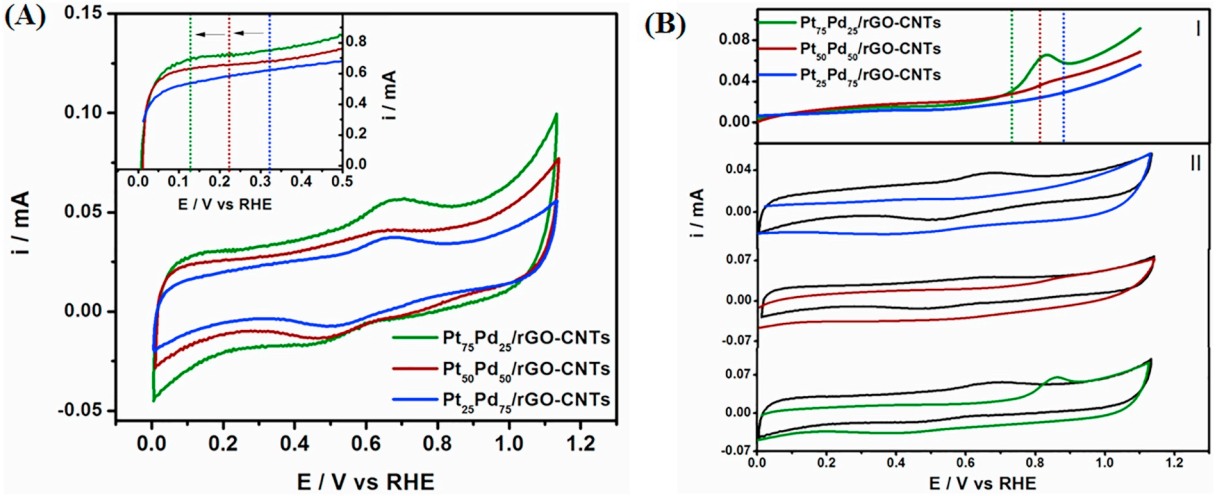

Fig. 5. Electrochemical CV and CO oxidation evaluation. (A) The characterization curves of electrochemical CV for all the PtPd alloys catalysts on rGO-CNTs, inset; showing the high magnification area for H_{upd} to show the shift in characteristic peak with different compositions of Pt with Pd and (B) the electrochemical CO oxidation/stripping curves for all the PtPd alloys series (I), full range CO oxidation CV along with base line (black color) CV of catalysts after the CO oxidation showing the exposed Hupd region that is unblocked after CO stripping (II).

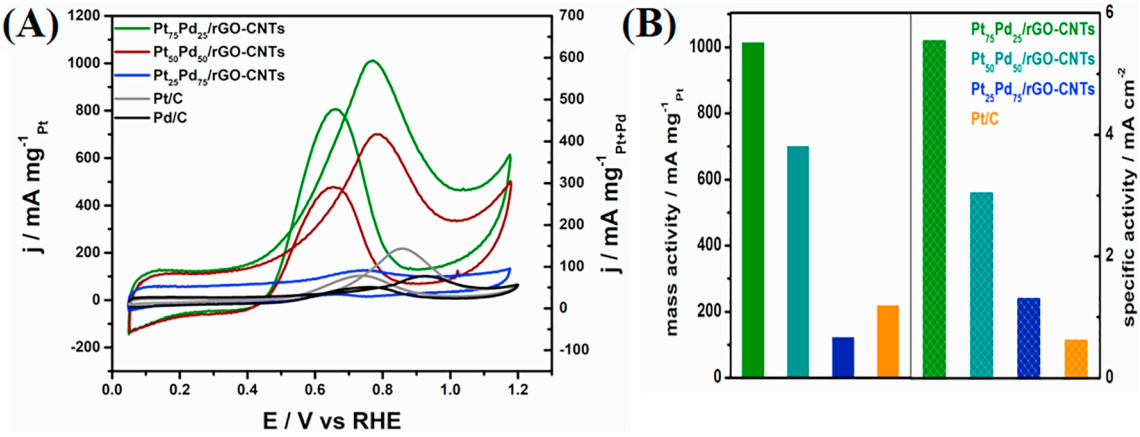

Fig. 6. Electrocatalytic MOR performance. (A) MOR performance of $Pt_{75}Pd_{25}$/rGO-CNTs, $Pt_{50}Pd_{50}$/rGO-CNTs, $Pt_{25}Pd_{75}$/rGO-CNTs and commercial 20 wt% Pt/C & Pd/C catalysts, in 0.1 M $HClO_4$ + 1 M CH_3OH at scan rate of 50 mV s^{-1} and (B) comparison of measured specific and mass activities at positive peak (If_{max}) potential for all catalysts compared with 20% Pt/C catalyst.

identification of the PtPd bimetallic alloys structures analyzed in the XRD and XPS studies. Furthermore, from these electrochemical CV curves, their electrochemical active surface areas (ECSAs) were calculated by integrating the area bounded by the H_{upd} curve region and the baseline in the range of 0.05–0.30 V (see Table S2). The ECSAs for the Pt based bimetallic alloys can be calculated by Q_H = mq, where "Q_H" is the total electric charge of hydrogen adsorption and desorption on the PtPd sites, "m" is the catalyst loading on the glassy carbon electrode (GCE) in gram (g) and the charge of each actual active area is assumed to be 210 mC cm^{-2} [50,51].

Carbon monoxide tolerance in methanol electro-oxidation catalysis is an important factor for developing efficient anode catalysts for fast chemisorptions of methanol [52]. In addition, the bifunctional mechanism in MOR can be easily convinced by explaining the process of CO electro-oxidation on catalysts surface. As the CO produced as intermediates species during methanol oxidation, block the active sites on the catalyst and stops further oxidation of methanol molecules into final product, thereby, decreasing the efficiency of overall DMFCs system.

It is believed that, CO species are extensively adsorbed on active sites of catalysts at lower potential values nearly below 0.40 V and hinders the adsorption of other carbonaceous species for chemisorptions. Hence, removal of these strongly adsorbed CO_{ads} from catalyst surface is an important task for quick and complete oxidation of methanol in DMFCs [53,54]. Herein, an enhanced performance of as-developed catalysts can be fairly explained by CO stripping experiments (see Fig. 5B). The obtained CO stripping voltammograms/curves showed the typical behavior, a projecting straight line with no H_{upd} peaks (presenting in black line base CVs for CO oxidation) with sudden inclined predicting the onset for CO oxidation over catalysts surfaces. It can also be seen from these results, there is a visible negative shift in CO oxidation onset potential with an increasing proportion of Pt in PtPd bimetallic alloys. These attainments in the CO oxidation experiments give a clear message for enhanced CO tolerance behavior that plays an important role for higher activity of present materials towards MOR.

The electrocatalytic performance for MOR was analyzed by electrochemical methods such as CVs in 0.1 M $HClO_4$ + 1 M CH_3OH solution and online differential electrochemical mass spectrometry (DEMS) for in-situ deep atomic level studies of methanol electro-oxidation. In MOR electrocatalysis system, there are few specified proposed mechanisms documented for the electro-oxidation of methanol on monometallic Pt and bimetallic Pt-based alloys catalysts [55–57]. The spectroscopic analysis coupled with potentiodynamic measurements of MOR has been recently introduced to unveil the atomic level step-by-step mechanistic assessments. It has been well-proposed that adsorption of methanol molecules on active Pt-sites are the primary step in MOR. Whereas, in secondary step CO_2 produces following the chemisorptions of surface adsorbed intermediates of methanol molecules via six electrons transfer phenomenon such as Pt-$(CHO)_{ads}$ and Pt$(CO)_{ads}$ [48,58,59]. Hence, the presence of co-element active sites in Pt-based (Pt-M) bimetallic alloys promotes the activation of water molecules to create Pt-$(OH)_{ads}$ and M-$(OH)_{ads}$ species those are reacting with the adsorbed carbonaceous intermediates species on Pt-sites to produce CO_2 as final product.

In typical CV trends of MOR there are two major peak curves, in the first forward scan anodic peak both the primary and secondary steps are involved such as, adsorption of carbonaceous species following the preparation of CO_2. Whereas, the second reverse scan peak correspond the further chemisorptions of surface adsorbed carbonaceous intermediates species to unblock pre-captured active sites. Among these, the Pt-$(CO)_{ads}$ are considered to be poisoning intermediates remain un-reacted and block the catalyst active sites for further MOR electrocatalysis. To assess the tolerance of these poisoning intermediates Pt-$(CO)_{ads}$ and enhanced activity during methanol electro-oxidation in Pt-based bimetallic catalysts, the ratio between forward anodic peak (I_f) to the backward anodic peak (I_b) have been calculated [60]. In this criterion, the higher I_f/I_b values represents that the secondary step in methanol oxidation is dominant to produce to the final product CO_2 showing negligible poisoning issue due to Pt-$(CO)_{ads}$ intermediates.

Herewith, the electrochemical CVs measurements for methanol oxidation were performed between 0.05 and 1.2 V vs RHE with a scan rate of 50 mV s^{-1}. As shown in (see Fig. 6A), all the CVs exhibit a typical MOR behavior with forward and backward scan peaks correspond to the electro-oxidation of methanol on catalysts surfaces. The forward scan exhibit that the oxidation of methanol happened at around 0.7 to 1.1 V following the removal of incompletely oxidized carbonaceous species in backward scan those produced during forward scan. The onset potential of MOR observed with shifting more towards negative scale from $Pt_{25}Pd_{75}$, $Pt_{50}Pd_{50}$ to $Pt_{75}Pd_{25}$ respectively. The observed MOR onset potentials for $Pt_{75}Pd_{25}$/rGO-CNTs at ca. ~0.35 V, $Pt_{50}Pd_{50}$/rGO-CNTs at ca. ~0.40 V and $Pt_{25}Pd_{75}$/rGO-CNTs at ca. ~0.53 V vs RHE appeared, predicting the shift in MOR onset potentials towards lower potential values with enhanced performance. The as-obtained onset potential also observed to be better than commercial 20 wt% Pt/C (with 0.60 V) and Pd/C catalysts. The peak current density values of specific and mass activities for all the bimetallic catalysts have shown the increasing trend of activities among $Pt_{25}Pd_{75}$ < $Pt_{50}Pd_{50}$ < $Pt_{75}Pd_{25}$ catalysts and as-well enhanced activities than that of commercial 20 wt% Pt/C catalyst (see Fig. 6B).

The understandings of higher MOR activities in present series of bimetallic PtPd catalysts supported on rGO-CNTs can be ascribed to

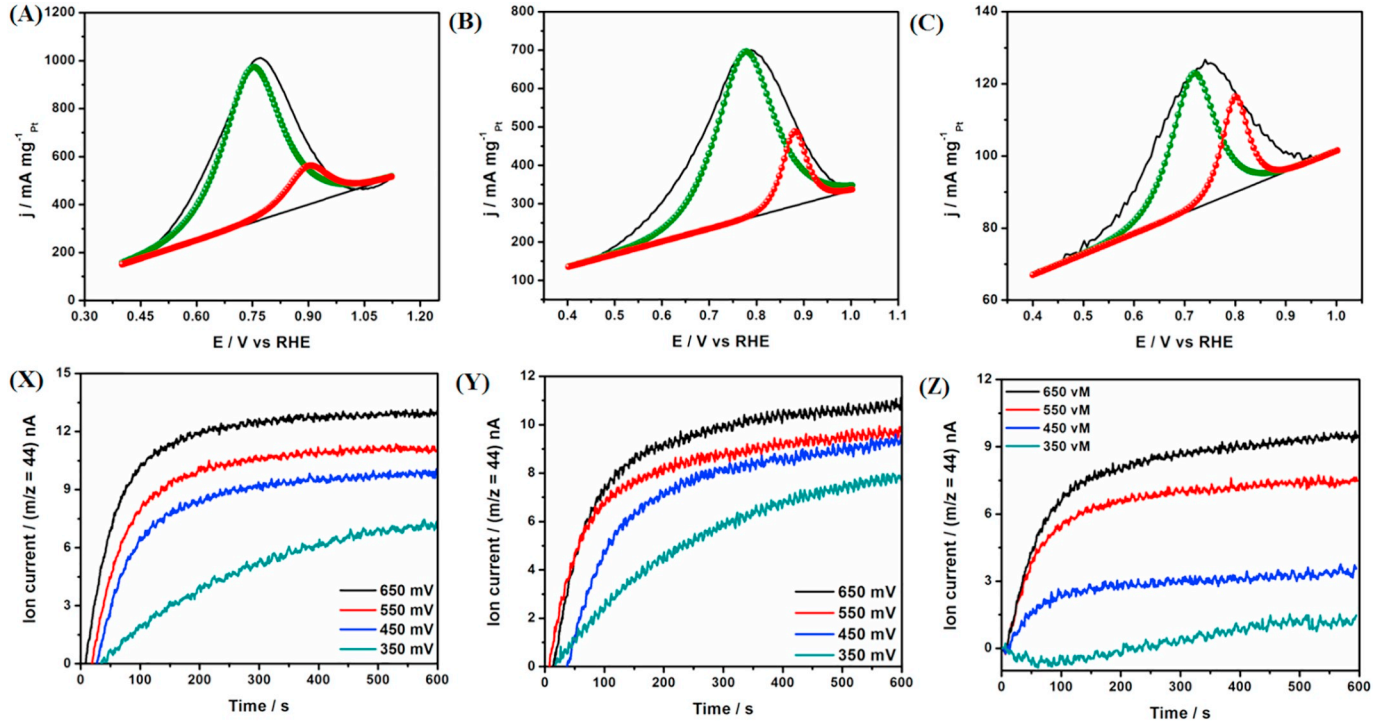

Fig. 7. MOR deconvolution analysis and online DEMS results for MOR. (A–C) Deconvolution of positive scan of MOR for $Pt_{75}Pd_{25}$/rGO-CNTs, $Pt_{50}Pd_{50}$/rGO-CNTs and $Pt_{25}Pd_{75}$/rGO-CNTs catalysts, respectively, divided by two peaks inside, the green colored peak predicting the proportion for direct intermediate pathway of MOR, whereas, the red colored peak proportion for indirect intermediate pathway, and (X–Z) online DEMS response of $Pt_{75}Pd_{25}$/rGO-CNTs, $Pt_{50}Pd_{50}$/rGO-CNTs and $Pt_{25}Pd_{75}$/rGO-CNTs catalysts, respectively, at four different applied potentials from 350 mV, 450 mV, 550 mV and 650 mV, time course of 600 s with reaction current and mass signal m/z = 44 from CO_2. (For interpretation of the references to color in this figure legend, the reader is referred to the web version of this article.)

various factors scientifically correlating with the construction of material. As stated above, the primary step of methanol oxidation is responsible for complete oxidation of methanol molecules via adsorption and chemisorptions of intermediate species into CO_2. This primary step further follows two possible routes, the direct and indirect oxidation of methanol [61,62]. In the first route, methanol is directly oxidized into CO_2 without experiencing CO poisoning and adsorption of un-reacted carbonaceous intermediates species issues. The direct oxidation oxidizes methanol to CO_2 directly. On the other hand, methanol molecules oxidized to CO via pre-adsorbed carbonaceous intermediates chemisorptions and later conversion into CO_2 by reacting with nearby $-OH_{ads}$ sites [61,62].

In present PtPd bimetallic alloys catalysts, the addition of Pd into Pt lowers the binding energy values of Pt, which is strongly verified and explained by XPS analysis, that weaken the association between CO and Pt-sites consequently lowered the CO poisoning on catalyst surface [62,63]. In addition, the bifunctional methanol oxidation mechanism, involves in PtPd bimetallic alloys catalysts. Herewith, the Pd-sites are responsible for the dehydrogenation of water molecules to produce Pd-OH_{ads}, in combination of above Pt-CO_{ads} weak association, these two species react with each other to prepare CO_2 leading towards the fast chemisorptions methanol. In this mechanism the transference of electrons play important role for quick oxidation of pre-adsorbed species, which is introduced by highly conductive rGO-CNTs support material in PtPd alloys through strong metal to support interactions. In this way the active sites on the surface of catalyst materials are also regained and catalyst became more efficient for further electro-oxidation of methanol molecules. As in case of excess Pd proportion the performance of catalyst decreased, it happened due to the unavailability of more Pt active sites in presence of higher Pd amount to adsorb more methanol molecules for oxidation. These three stated phenomenon (i) weak Pt and CO binding associations, (ii) bifunctional MOR mechanism in PtPd and (iii) electrons transference phenomenon due to conductive support highly enhanced the indirect route of oxidation process during methanol electro-oxidation [27].

Moreover, there are also possibilities for direct route of methanol oxidation in present series of catalysts that enhanced the performance of catalysts due to the following proposed facts. The downshifting of Pt binding energies also possibly reduces the adsorption of CO_{ads} species on its surface and following the direct oxidation of adsorbed methanol molecules without producing CO_{ads} intermediates [64]. The facet effects are also accountable to support the high performance of catalysts linked with direct rout of oxidation such as, high index surfaces of the Pt (111) present in these PtPd bimetallic alloys those are verified and explained above by HRTEM and XRD characterizations, which can accelerate the electrocatalytic activities of catalysts [65]. These Pt (111) facets strongly inhibit the adsorption of CO molecules on its surface, hence following the direct route of methanol oxidation with chemisorptions of adsorbed methanol molecules [62].

The mechanism of MOR is further confirmed by deconvolution of positive scans for all the catalysts to show the proportions related to direct oxidation or dehydrogenation mechanism and the indirect oxidation routes, shown in Fig. 7A–C. The deconvoluted positive scans of each catalysts contains two inset peaks, the green colored peak and the red colored peak correspond to direct and indirect intermediates pathways of methanol electro-oxidation respectively. It can be clearly shown the peak area and intensity for direct pathways are comparatively reducing from $Pt_{75}Pd_{25}$/rGO-CNTs, $Pt_{50}Pd_{50}$/rGO-CNTs to $Pt_{25}Pd_{75}$/rGO-CNTs. On the other hand, the indirect or poisoning intermediate peak intensity and proportion is increasing with same trend. These electrochemical screening confirm the superiority of $Pt_{75}Pd_{25}$/rGO-CNTs over the other materials due to the fact that poisoning intermediates routes are diminishing and the MOR performance is enhancing by following a direct chemisorptions pathway through an active intermediate routes [64]. Moreover, the superiority of present catalyst material towards MOR have also compared with the state-of-

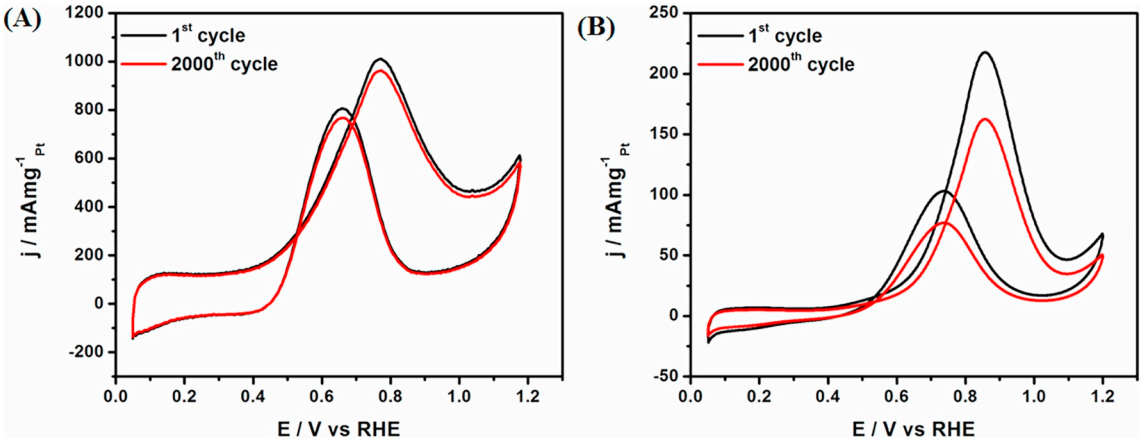

Fig. 8. Accelerated durability test (ADTs) for MOR activity. (A) ADTs results of $Pt_{75}Pd_{25}$/rGO-CNTs catalyst and (B) ADTs results of commercial 20 wt% Pt/C, in N_2 saturated 0.1 M $HClO_4$ + 1 M CH_3OH with 100 mV s^{-1} scan rate.

the-art Pt-based catalysts already reported by the different groups, the comparison table is provided in Table S3.

In addition, the online DEMS studies have also done for all the catalysts at different potentials of 0.35 V, 0.45 V, 0.55 V and 0.65 V, time course of 600 s with reaction current and mass signal $m/z = 44$ from CO_2. These featured results revealed the production of final product CO_2 during methanol electro-oxidation. DEMS is a strong electrochemical characterization tool for the analysis of volatile products formation during methanol electro-oxidation on the surface of catalysts [66,67]. The atomic level evaluation of catalysts in MOR performance performed by online DEMS exhibit the formation of CO_2 with a linearly increased signals of mass spectrometric ($m/z = 44$) ion current signals (those converted into a partial Faradic current for CO_2) [66] by increasing potential values following the complete oxidation of methanol in all the bimetallic alloys catalysts (see Fig. 7X–Z).

These results are useful to unveil the efficiency of electrocatalysts by analyzing the complete oxidation reaction for fuels, by the mass spectrometric ($m/z = 44$) ion current signals converted into a partial Faradic current for CO_2 [68]. As the complete oxidation of methanol molecules follow the six electrons transfer reaction. To find out the current signals related to CO_2 means there is a successful oxidation of methanol on catalyst surface to form the end product. The findings confirm the fast chemisorptions of methanol assuming the concepts of six electrons ($n = 6$) released/transferred reaction per CO_2 molecule produced from methanol. The observed DEMS results exhibit CO_2 ion currents were increased linearly by increasing the potential during methanol oxidation, following the potential step, at first the CO_2 ion currents increased and then achieved a plateau value within a specified period of time and then remained constant. These outcomes also reflect the complete and fast oxidation of methanol leaving behind no residual adsorbed species on the surface of catalysts those are not reacted during oxidation reaction.

Moreover, the durable nature of methanol electro-oxidation on present materials was also analyzed by electrochemical accelerated durability tests (ADTs). These ADTs were employed on higher performance $Pt_{75}Pd_{25}$/rGO-CNTs catalyst in comparison with commercial 20 wt% Pt/C catalyst to evaluate the long-term performance and stability of the catalysts. The durability was presented in terms of loadings of metals, which can also suggest the enhanced and durable performance of catalysts with their highly stable chemical behavior. The ADTs results shown (see Fig. 8A & B) the $Pt_{75}Pd_{25}$/rGO-CNTs catalyst experienced a loss of approximately 2.1%, while, the commercial Pt/C catalyst lost 26.8% after 2000 cycles of methanol electro-oxidation. The loss of MOR performance is ascribed to the corrosion of the carbon support material in the catalyst, the subsequent agglomeration and leaching of metallic NPs have been documented as the major factor for the decrease in MOR performance [45]. In case of durable performance of $Pt_{75}Pd_{25}$/rGO-CNTs catalyst over Pt/C mainly acknowledging the corrosion resistant, highly conducive carbon-based support material such as, rGO-CNTs to provide stable dispersion of metallic alloys NPs with durable performance.

4. Conclusions

In conclusions, we have been successful in developing highly active anode catalysts for DMFCs with a series of tuned compositions such as, $Pt_{75}Pd_{25}$/rGO-CNTs, $Pt_{50}Pd_{50}$/rGO-CNTs and $Pt_{25}Pd_{75}$/rGO-CNTs. The powerful catalytic behavior of both the metals Pt and Pd in combination with highly conductive and synergistic rGO-CNTs support material shown enhanced and durable performance for MOR. The HRTEM analysis correlating with electrochemical characterizations predicts the major proportions of Pt (111) facets sharing the same geometries with its partner element highly introduced the CO tolerance characteristics in catalysts, later confirmed by CO stripping results. The structural XPS and XRD analysis revealed the strong mutual electrons transference phenomenon among metallic alloys and the support, which facilitated the fast chemisorptions of methanol molecules by following the direct or active intermediates pathways. The highly convincing results obtained from online DEMS further supported the stated claims, as by increasing the potential values during MOR increased the amount of CO_2 produced during reactions. The overall outcomes suggested the fast and durable methanol electro-oxidation of as-developed anode catalyst for DMFCs and open up effective routes strategies for developing active materials in the avenue of renewable energy applications.

Authors contributions

A. B. Y. and M. I. contributed equally to this work.

Notes

The authors declare no competing financial interest.

Acknowledgement

The authors acknowledge financial support from the Qatar National Research Fund (A Member of The Qatar Foundation) NPRP grant #9-219-2-105. This work is also supported by the CAS-TWAS Presidents Fellowship Programme, USTC and Anhui Government Scholarship programmes. The statements made herein are solely the responsibility of the authors.

Appendix A. Supplementary data

Supplementary data to this article can be found online at https://doi.org/10.1016/j.jelechem.2018.11.033.

References

[1] V.R. Stamenkovic, B. Fowler, B.S. Mun, G. Wang, P.N. Ross, C.A. Lucas, N.M. Markovic, Improved oxygen reduction activity on Pt3Ni (111) via increased surface site availability, Science 315 (2007) 493–497.

[2] S. Guo, S. Zhang, S. Sun, Tuning nanoparticle catalysis for the oxygen reduction reaction, Angew. Chem. Int. Ed. 52 (2013) 8526–8544.

[3] D.F. Van der Vliet, C. Wang, D. Tripkovic, D. Strmcnik, X.F. Zhang, M.K. Debe, R.T. Atanasoski, N.M. Markovic, V.R. Stamenkovic, Mesostructured thin films as electrocatalysts with tunable composition and surface morphology, Nat. Mater. 11 (2012) 1051–1058.

[4] D.F. Van der Vliet, C. Wang, D. Li, A.P. Paulikas, J. Greeley, R.B. Rankin, D. Strmcnik, D. Tripkovic, N.M. Markovic, V.R. Stamenkovic, Unique electrochemical adsorption properties of Pt-skin surfaces, Angew. Chem. 124 (2012) 3193–3196.

[5] J. Erlebacher, M.J. Aziz, A. Karma, N. Dimitrov, K. Sieradzki, Evolution of nanoporosity in dealloying, Nature 410 (2001) 450–453.

[6] B.C. Steele, A. Heinzel, Materials for fuel-cell technologies, Nature 414 (2001) 345–352.

[7] Z.Y. Shih, C.W. Wang, G. Xu, H.T. Chang, Porous palladium copper nanoparticles for the electrocatalytic oxidation of methanol in direct methanol fuel cells, Mater. Chem. A 1 (2013) 4773–4778.

[8] Y. Zhao, J. Liu, C. Liu, F. Wang, Y. Song, Amorphous CuPt alloy nanotubes induced by $Na_2S_2O_3$ as efficient catalysts for the methanol oxidation reaction, ACS Catal. 6 (2016) 4127–4134.

[9] X. Du, S. Luo, H. Du, M. Tang, X. Huang, P.K. Shen, Monodisperse and self-assembled Pt-Cu nanoparticles as an efficient electrocatalyst for the methanol oxidation reaction, J. Mater. Chem. A 4 (2016) 1579–1585.

[10] D. Chen, Y. Zhao, X. Peng, X. Wang, W. Hu, C. Jing, S. Tian, J. Tian, Star-like PtCu nanoparticles supported on graphene with superior activity for methanol electrooxidation, Electrochim. Acta 177 (2015) 86–92.

[11] D. Wang, H.L. Xin, R. Hovden, H. Wang, Y. Yu, D.A. Muller, F.J. DiSalvo, H.D. Abrun, Structurally ordered intermetallic platinum-cobalt core-shell nanoparticles with enhanced activity and stability as oxygen reduction electrocatalysts, Nat. Mater. 12 (2012) 81–87.

[12] C. Wang, M. Chi, D. Li, D. Strmcnik, D. Van der Vliet, G. Wang, V. Komanicky, K.C. Chang, A.P. Paulikas, D. Tripkovic, Design and synthesis of bimetallic electrocatalyst with multilayered Pt-skin surfaces, J. Am. Chem. Soc. 133 (2011) 14396–14403.

[13] S. Koh, P. Strasser, Electrocatalysis on bimetallic surfaces: modifying catalytic reactivity for oxygen reduction by voltammetric surface dealloying, J. Am. Chem. Soc. 129 (2007) 12624–12625.

[14] J. Wu, H. Yang, Platinum-based oxygen reduction electrocatalysts, Acc. Chem. Res. 46 (2013) 1848–1857.

[15] X.J. Wan, Y. Huang, Y.S. Chen, Focusing on energy and optoelectronic applications: a journey for graphene and graphene oxide at large scale, Acc. Chem. Res. 45 (2012) 598–607.

[16] X. Huang, X.Y. Qi, F. Boey, H. Zhang, Graphene-based composites, Chem. Soc. Rev. 41 (2012) 666–686.

[17] A.B. Yousaf, M. Imran, S.J. Zaidi, P. Kasak, T.M. Ansari, S. Manzoor, G. Yasmeen, Synergistic effect of interfacial phenomenon on enhancing catalytic performance of Pd loaded MnO_x-CeO_2-C hetero-nanostructure for hydrogenation and electrochemical reactions, J. Mater. Chem. A 5 (2017) 10704–10712.

[18] Z.J. Fan, J. Yan, L.J. Zhi, Q. Zhang, T. Wei, J. Feng, M.L. Zhang, W.Z. Qian, F. Wei, A three-dimensional carbon nanotube/graphene sandwich and its application as electrode in supercapacitors, Adv. Mater. 22 (2010) 3723–3728.

[19] V.C. Tung, L.M. Chen, M.J. Allen, J.K. Wassei, K. Nelson, R.B. Kaner, Y. Yang, Low-temperature solution processing of graphene−carbon nanotube hybrid materials for high-performance transparent conductors, Nano Lett. 9 (2009) 1949–1955.

[20] G.Q. Xin, W.H. Wang, N. Kim, S.M. Cho, H. Chae, A graphene sheet exfoliated with microwave irradiation and interlinked by carbon nanotubes for high-performance transparent flexible electrodes, Nanotechnology 21 (2010) 405201.

[21] E.J. Yoo, J.D. Kim, E.J. Hosono, H.S. Zhou, T. Kudo, I. Honma, Large reversible li storage of graphene nanosheet families for use in rechargeable lithium ion batteries, Nano Lett. 8 (2008) 2277–2282.

[22] K.P. Loh, Q.L. Bao, G. Eda, M. Chhowalla, Graphene oxide as a chemically tunable platform for optical applications, Nat. Chem. 2 (2010) 1015–1024.

[23] K. Moon, J. Lee, R.S. Ruoff, H. Lee, Reduced graphene oxide by chemical graphitization, Nat. Commun. 1 (2010) 73.

[24] M. Khan, A.B. Yousaf, M.M. Chen, C.S. Wei, X. Wu, N.D. Huang, Z.M. Qi, L.B. Li, Molybdenum sulfide/graphene-carbon nanotube nanocomposite material for electrocatalytic applications in hydrogen evolution reactions, Nano Res. 9 (2016) 837–848.

[25] Y. Zhou, Q.L. Bao, L.A.L. Tang, Y.L. Zhong, K.P. Loh, Hydrothermal dehydration for the “green” reduction of exfoliated graphene oxide to graphene and demonstration of tunable optical limiting properties, Chem. Mater. 21 (2009) 2950–2956.

[26] S.D. Seo, I.S. Hwang, S.H. Lee, H.W. Shim, D.W. Kim, 1D/2D carbon nanotube/graphene nanosheet composite anodes fabricated using electrophoretic assembly, Ceram. Int. 38 (2012) 3017–3021.

[27] Y. Liu, M.F. Chi, V. Mazumder, K.L. More, S. Soled, J.D. Henao, S.H. Sun, Composition-controlled synthesis of bimetallic PdPt nanoparticles and their electro-oxidation of methanol, Chem. Mater. 23 (2011) 4199–4203.

[28] F.W. Zhan, T. Bian, W.G. Zhao, H. Zhang, M.S. Jin, D. Yanga, Facile synthesis of Pd–Pt alloy concave nanocubes with high-index facets as electrocatalysts for methanol oxidation, CrystEngComm 16 (2014) 2411–2416.

[29] Y. Kim, Y. Noh, E.J. Lim, S. Lee, S.M. Choi, W.B. Kim, Star-shaped Pd@Pt core–shell catalysts supported on reduced graphene oxide with superior electrocatalytic performance, J. Mater. Chem. A 2 (2014) 6976–6986.

[30] G.H. Yang, Y.Z. Zhou, H.B. Pan, C.Z. Zhu, S.F. Fu, C.M. Wai, D. Du, J.J. Zhu, Y. Lin, Ultrasonic-assisted synthesis of Pd–Pt/carbon nanotubes nanocomposites for enhanced electro-oxidation of ethanol and methanol in alkaline medium, Ultrason. Sonochem. 28 (2016) 192–198.

[31] W.S.Jr. Hummers, R.E. Offeman, Preparation of graphitic oxide, J. Am. Chem. Soc. 80 (1958) 1339.

[32] A.B. Yousaf, M. Imran, A. Zeb, W. Tao, X. Xiao, Y.F. Jiang, C.Z. Yuan, A.W. Xu, Single phase PtAg bimetallic alloy nanoparticles highly dispersed on reduced graphene oxide for electrocatalytic application of methanol oxidation reaction, Electrochim. Acta 197 (2016) 117–125.

[33] K. Sasaki, H. Naohara, Y. Cai, Y. Choi, P. Liu, M. Vukmirovic, J. Wang, R. Adzic, Core-protected platinum monolayer shell high-stability electrocatalysts for fuel-cell cathodes, Angew. Chem. Int. Ed. 49 (2010) 8602–8607.

[34] J. Datta, A. Dutta, S. Mukherjee, The beneficial role of the cometals Pd and Au in the carbon-supported PtPdAu catalyst toward promoting ethanol oxidation kinetics in alkaline fuel cells: temperature effect and reaction mechanism, J. Phys. Chem. C 115 (2011) 15324–15334.

[35] Y. Zhang, G. Chang, H. Shu, M. Oyama, X. Liu, Y. He, Synthesis of Pt–Pd bimetallic nanoparticles anchored on graphene for highly active methanol electro-oxidation, J. Power Sources 262 (2014) 279–285.

[36] K. Chang, W.X. Chen, In situ synthesis of MoS_2/graphene nanosheet composites with extraordinarily high electrochemical performance for lithium ion batteries, Chem. Commun. 47 (2011) 4252–4254.

[37] Y. Wang, Q.L. He, H. Wei, J. Guo, K.Q. Ding, Q. Wang, Z. Wang, S. Wei, Z.H. Guo, Optimal electrocatalytic Pd/MWNTs nanocatalysts toward formic acid oxidation, Electrochim. Acta 184 (2015) 452–465.

[38] T.I.T. Okpalugo, P. Papakonstantinou, H. Murphy, J. McLaughlin, N.M.D. Brown, High resolution XPS characterization of chemical functionalised MWCNTs and SWCNTs, Carbon 43 (2005) 153–161.

[39] K.R. Lee, K.U. Lee, J.W. Lee, B.T. Ahn, S.I. Woo, Electrochemical oxygen reduction on nitrogen doped graphene sheets in acid media, Electrochem. Commun. 12 (2010) 1052–1055.

[40] A. Scibioh, S. Kim, E.A. Cho, T.H. Lim, S.A. Hong, H.Y. Ha, Pt-CeO_2/C anode catalyst for direct methanol fuel cells, Appl. Catal. B 84 (2008) 773–782.

[41] X. Huang, H. Zhang, C. Guo, Z. Zhou, N. Zheng, Simplifying the creation of hollow metallic nanostructures: one-pot synthesis of hollow palladium/platinum single-crystalline nanocubes, Angew. Chem. Int. Ed. 48 (2009) 4808–4812.

[42] S. Wasmus, J.T. Wang, R.F. Savinell, Real time mass spectrometric investigation of the methanol oxidation in a direct methanol fuel cell, J. Electrochem. Soc. 142 (1995) 3825−−3833.

[43] X. Han, T. Zhang, J. Du, F. Cheng, J. Chen, Porous calcium manganese oxide microspheres for electrocatalytic oxygen reduction with high activity, Chem. Sci. 4 (2013) 368–376.

[44] Z.Y. Sun, X. Wang, Z.M. Liu, H. Zhang, P. Yu, L.Q. Mao, Pt-Ru/CeO_2/carbon nanotube nanocomposites: an efficient electrocatalyst for direct methanol fuel cells, Langmuir 26 (2010) 12383–12389.

[45] Y. Lu, Y. Jiang, H. Wu, W. Chen, Nano-PtPd cubes on graphene exhibit enhanced activity and durability in methanol electrooxidation after CO stripping–cleaning, J. Phys. Chem. C 117 (2013) 2926–2938.

[46] K.W. Park, J.H. Choi, B.K. Kwon, S.A. Lee, Y.E. Sung, H.Y. Ha, S.A. Hong, H. Kim, A. Wieckowski, Chemical and electronic effects of Ni in Pt/Ni and Pt/Ru/Ni alloy nanoparticles in methanol electrooxidation, J. Phys. Chem. B 106 (2002) 1869–1877.

[47] F.J. Vidal-Iglesias, R.M. Arán-Ais, J. Solla-Gullón, E. Herrero, J.M. Feliu, Electrochemical characterization of shape-controlled Pt nanoparticles in different supporting electrolytes, ACS Catal. 2 (2012) 901–910.

[48] K. Mikkelsen, B. Cassidy, N. Hofstetter, H. Bergquist, A. Taylor, D.A. Rider, Block copolymer templated synthesis of core–shell PtAu bimetallic nanocatalysts for the methanol oxidation reaction, Chem. Mater. 26 (2014) 6928–6940.

[49] C. Wang, D. Van der Vliet, K.L. More, N.J. Zaluzec, S. Peng, S. Sun, H. Daimon, G. Wang, J. Greeley, J. Pearson, A.P. Paulikas, G. Karapetrov, D. Strmcnik, N.M. Markovic, V.R. Stamenkovic, Multimetallic Au/$FePt_3$ nanoparticles as highly durable electrocatalyst, Nano Lett. 11 (2011) 919–926.

[50] H. Ye, R.M. Crooks, Effect of elemental composition of PtPd bimetallic nanoparticles containing an average of 180 atoms on the kinetics of the electrochemical oxygen reduction reaction, J. Am. Chem. Soc. 129 (2007) 3627–3633.

[51] Y. Xiong, H. Cai, B. Wiley, J. Wang, M. Kim, Y. Xia, Synthesis and mechanistic study of palladium nanobars and nanorods, J. Am. Chem. Soc. 127 (2007) 3665–3675.

[52] F. Maillard, E.R. Savinova, U. Stimming, CO monolayer oxidation on Pt nanoparticles: further insights into the particle size effects, J. Electroanal. Chem. 599 (2007) 221–232.

[53] P.H.C. Camargo, Y.J. Xiong, L. Ji, J.M. Zuo, Y. Xia, Facile synthesis of tadpole-like nanostructures consisting of au heads and Pd tails, J. Am. Chem. Soc. 129 (2007) 15452–15453.

[54] T.M. Koper, A.P.J. Jansen, Monte Carlo simulations of a simple model for the electrocatalytic co oxidation on platinum, J. Chem. Phys. 109 (1998) 6051–6062.

[55] L. Wang, F. Montagne, P. Hoffmann, R. Pugin, Gold nanoring arrays from

responsive block copolymer templates, Chem. Commun. (2009) 3798–3800.
[56] W.H. Zhong, Y.X. Liu, D.J. Zhang, Theoretical study of methanol oxidation on the PtAu(111) bimetallic surface: CO pathway vs non-CO pathway, J. Phys. Chem. C 116 (2012) 2994–3000.
[57] A.K. Singh, Q. Xu, Synergistic catalysis over bimetallic alloy nanoparticles, Chem. Catal. Chem. 5 (2013) 652–676.
[58] Z.L. Liu, X.Y. Ling, X.D. Su, J.Y. Lee, Carbon-supported Pt and PtRu nanoparticles as catalysts for a direct methanol fuel cell, J. Phys. Chem. B 108 (2004) 8234–8240.
[59] M.S. She, T.Y. Lo, H.Y. Hsueh, R.M. Ho, Nanostructured thin films of degradable block copolymers and their applications, NPG Asia Mater. 5 (2013) e42.
[60] H. Turner, A.M. Single, Determination of peak positions and areas from wide-scan XPS spectra, Surf. Interface Anal. 15 (1990) 215–222.
[61] S. Sharma, A. Ganguly, P. Papakonstantinou, X. Miao, M. Li, J.L. Hutchison, M. Delichatsios, S. Ukleja, Rapid microwave synthesis of CO tolerant reduced graphene oxide-supported platinum electrocatalysts for oxidation of methanol, J. Phys. Chem. C 114 (2010) 19459–19466.
[62] L.F. Lu, S. Chen, S. Thota, X.D. Wang, Y.C. Wang, S.H. Zou, J. Fan, J. Zhao, Composition controllable synthesis of PtCu nanodendrites with efficient electrocatalytic activity for methanol oxidation induced by high index surface and electronic interaction, J. Phys. Chem. C 121 (2017) 19796–19806.
[63] J. Zhang, K. Li, B. Zhang, Synthesis of dendritic Pt-Ni-P alloy nanoparticles with enhanced electrocatalytic properties, Chem. Commun. 51 (2015) 12012–12015.
[64] R. Bavand, Q. Wei, G. Zhang, S. Sun, A. Yelon, E. Sacher, PtRu alloy nanoparticles. 2. Chemical and electrochemical surface characterization for methanol oxidation, J. Phys. Chem. C 121 (2017) 23120–23128.
[65] B.Y. Xia, H.B. Wu, X. Wang, X.W.D. Lou, Highly concave platinum nanoframes with high-index facets and enhanced electrocatalytic properties, Angew. Chem. Int. Ed. 52 (2013) 12337–12340.
[66] J. Willsau, O. Wolter, J. Heitbaum, On the nature of the adsorbate during methanol oxidation at platinum: a DEMS study, J. Electroanal. Chem. Interfacial Electrochem. 185 (1985) 163–170.
[67] J. Willsau, J. Heitbaum, Analysis of adsorbed intermediates and determination of surface potential shifts by dems, Electrochim. Acta 31 (1986) 943–948.
[68] M.C. Halseid, Z. Jusys, R.J. Behm, Methanol oxidation over a Pt/C catalyst at high temperatures and pressure: an online electrochemical mass spectrometry study, J. Phys. Chem. C 114 (2010) 22573–22581.